ORIGINAL RESEARCH

Chaihuang Qingfu Pills Protect Against Acute Pancreatitis—Associated Acute Lung Injury Through MMP9-NLRP3-Pyroptosis Pathway

Wen Xiao [1–3],*, Huiying Shi[1,2],*, Yuan Tian[4], Fang Chen[1–3], Yuanzhu Xie[1,2], Xiaotong Han[1,2], Xingwen Zhang[1,2], Yan Cao[1,2], Wen Liu[1,2], Yimin Zhu[1,2], Yanjuan Liu[1,2], Yu Jiang[1,2]

[1]Institute of Emergency Medicine, Department of Emergency, the First Affiliated Hospital of Hunan Normal University (Hunan Provincial People's Hospital), Changsha, Hunan, People's Republic of China; [2]Hunan Provincial Key Laboratory of Emergency and Critical Care Metabonomics, Changsha, Hunan, People's Republic of China; [3]Department of Physiology, College of Life Sciences, Hunan Normal University, Changsha, Hunan, People's Republic of China; [4]Clinical School of Medicine, Hunan University of Chinese Medicine, Changsha, Hunan, People's Republic of China

*These authors contributed equally to this work

Correspondence: Yu Jiang; Yanjuan Liu, Institute of Emergency Medicine, Department of Emergency, the First Affiliated Hospital of Hunan Normal University (Hunan Provincial People's Hospital), Fu-Rong District, Changsha City, Hunan Province, 410005, People's Republic of China, Email jiangyu@hunnu.edu.cn; liuyanjuan@hunnu.edu.cn

Background: Severe acute pancreatitis associated with acute lung injury (SAP-ALI) is a critical condition with a high mortality rate. Investigating the pathogenesis of SAP-ALI and developing effective treatments are urgently needed. Chaihuang Qingfu Pills (CHQF), a traditional Chinese medicine modified from Qingyi Decoction, has been approved for treating acute pancreatitis (AP). However, its role in SAP-ALI and the underlying mechanisms remain unclear.
Methods: 92 AP patients were enrolled to observe the protective effect of CHQF on AP-ALI. L-arginine was used to establish the SAP-ALI animal model. UHPLC-MS/MS was used to identify the components of CHQF absorbed into the serum. Transcriptomics analysis, network pharmacology, and proteomics approaches were used to explore the underlying molecular mechanism. In vivo and in vitro experiments were conducted to validate the relevant findings.
Results: Clinical data indicated CHQF reduced the incidence of ALI from 58.33% to 36.36% in AP patients. Animal experiments demonstrated that CHQF decreased mortality, attenuated organ damage, inhibited systemic inflammation and reduced pathological injury in SAP mice. Differential expression analysis and weighted gene co-expression network analysis (WGCNA) identified 146 SAP-related differentially expressed genes (DEGs) from the GSE194331 dataset. UHPLC-MS/MS analysis acquired 26 components absorbed into the blood and 271 associated therapeutic targets. Integrated analysis obtained 52 core targets of CHQF in treating SAP. Proteomic analysis identified 216 proteins associated with CHQF treatment in SAP-ALI. Joint analysis found that MMP9 and NLRP3 were the only common targets. Both in vivo and in vitro experiments confirmed that CHQF reduced the levels of MMP9 and NLRP3 and inhibited pyroptosis in alveolar macrophages (AMs) under SAP conditions. Moreover, the MMP9 inhibitor reduced NLRP3 expression and suppressed AMs pyroptosis.
**Conclusion:** CHQF exerted a protective role in SAP-ALI by inhibiting macrophage pyroptosis through the MMP9-NLRP3 pathway, providing a novel therapeutic strategy for SAP-ALI.
Keywords: chaihuang qingfu pills, severe acute pancreatitis, acute lung injury, MMP9, NLRP3, pyroptosis

Introduction

Acute pancreatitis (AP) is an inflammatory disease caused by the abnormal activation of digestive enzymes, which can progress to systemic inflammatory response syndrome (SIRS) and multiple organ dysfunction syndrome (MODS).[1] Acute lung injury (ALI), characterized by inflammation and impaired gas exchange, occurs in up to 55% of AP patients.[1–3] Severe acute pancreatitis-associated ALI (SAP-ALI) is a major cause of early mortality in SAP, contributing to up to 60% of SAP-related deaths.[4,5] Despite improvements in critical care, effective treatments for SAP-ALI remain

Graphical Abstract
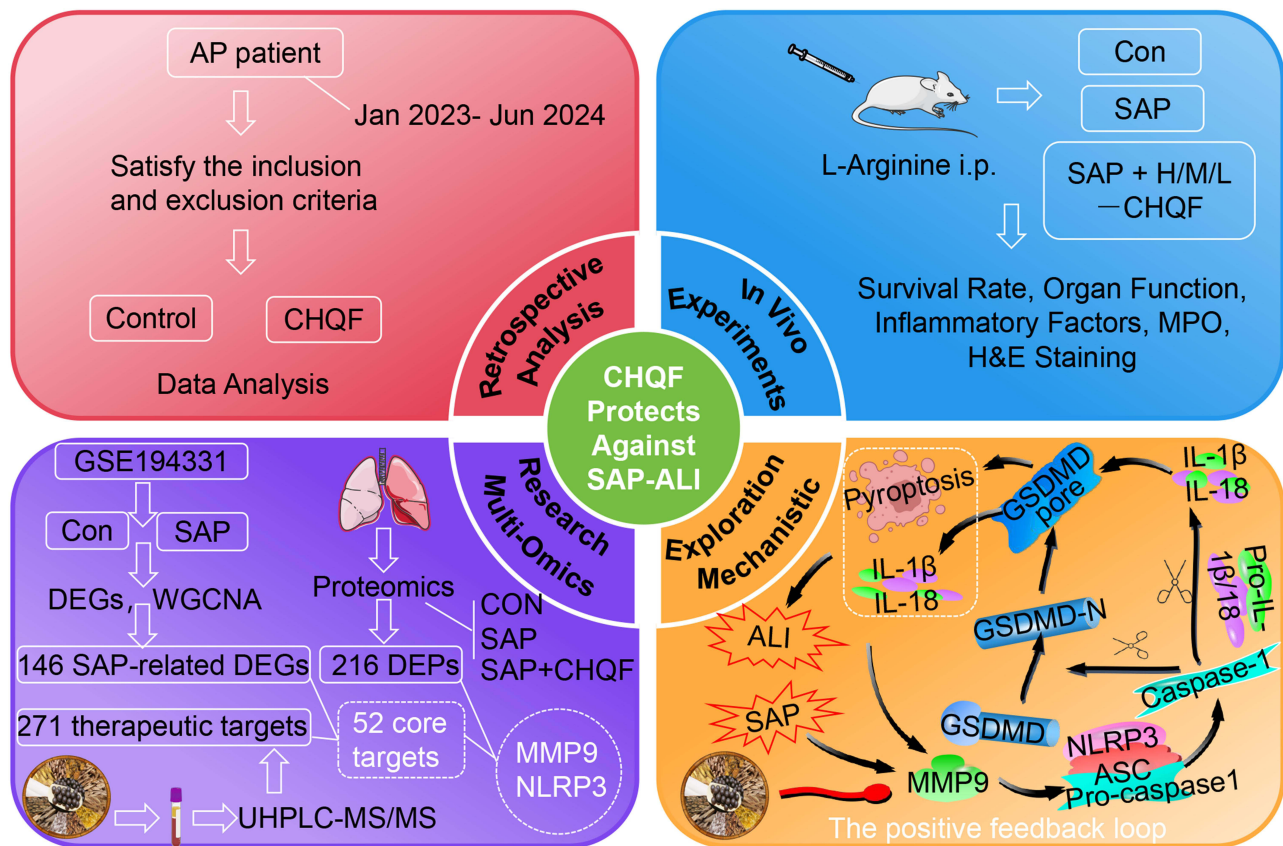
limited, and its underlying mechanisms are poorly understood.[6,7] This underscores the urgent need for further research to elucidate the pathophysiology of SAP-ALI and develop novel therapeutic strategies.

Chaihuang Qingfu Pills (CHQF), is a new drug modified from the classic prescription Qingyi Decoction, with the dosage form changed from decoction to pill. Qingyi Decoction has been garnered significant attention for its therapeutic efficacy in treating AP.[6,8–10] Traditional Chinese Medicine (TCM) holds that Qingyi Decoction has robust efficacy in clearing heat and detoxifying, as well as soothing the liver and promoting bile secretion and flow.[8] Modern pharmacological researches suggest that Qingyi Decoction has multiple bioactivities, such as anti-inflammatory and immunomodulatory effects, inhibition of pancreatic enzyme secretion, and improvement in organ microcirculation.[9–11] Comprising twelve medicinal materials — Bupleurum chinense DC, Scutellaria baicalensis Georgi, Rheum officinale Baill, Picrorhiza scrophulariiflora Pennell, Dictamnus dasycarpus Turcz, Aucklandia lappa Decne, Lonicera japonica, Forsythia suspensa, Paeonia lactiflora Pall, Citrus aurantium, Houpoea officinalis, and thenardite (all plant names have been checked with http://www.theplantlist.org/) — CHQF presents advantages in standardized production, convenient administration, and a stable composition compared to Qingyi Decoction, and has demonstrated certain clinical efficacy. However, the material basis for its therapeutic effects following oral administration and serum absorption, as well as its distinct roles in the pathogenesis of SAP-ALI and underlying mechanisms, remain unclear.

In the current work, we aimed to assess the protective effect of CHQF in SAP-ALI and explore its potential mechanism. Firstly, 92 AP patients were enrolled to investigate the clinical efficacy of CHQF. Subsequently, an SAP-ALI animal model was established using L-arginine. Ultrahigh Performance Liquid Chromatography-Mass Spectrometry/Mass Spectrometry (UHPLC-MS/MS), transcriptomics analysis, network pharmacology, and proteomics

approaches were used to explore the exact molecular mechanism. Our findings revealed that MMP9 and NLRP3 were the crucial targets of CHQF in attenuating SAP-ALI. Moreover, in vivo and in vitro experiments confirmed that CHQF alleviated SAP-ALI by inhibiting macrophage pyroptosis through the MMP9-NLRP3 pathway, thereby providing a theoretical foundation for its further clinical promotion.

Methods

Patients

A total of 92 AP patients, aged 18–70 years, who were hospitalized at Hunan Provincial People's Hospital within 48 hours of symptom onset between January 2023 and June 2024, were enrolled. All AP patients satisfied the criteria outlined in the Atlanta Classification and Definition of Acute Pancreatitis (2012). The diagnosis of ALI was based on the Berlin definition. Exclusion criteria included patients who had received other traditional Chinese medicines similar to CHQF, had a history of emphysema, chronic obstructive pulmonary disease (COPD), chronic pneumonia, lung cancer, or exhibited pneumonia symptoms prior to the onset of AP. Additionally, those who were pregnant or patients with severe comorbidities that could complicate the assessment of SAP-ALI were also excluded. Patients were treated according to the "Guidelines for diagnosis and treatment of acute pancreatitis in China (2021)".[12] Those who received standard treatment according to the guidelines were assigned to the control group, while patients who, in addition to standard treatment, received CHQF as per the physician's prescription were assigned to the CHQF group.

Animals

A total of 150 specific pathogen-free (SPF) adult male BALB/c mice (6–8 weeks old, weighing 18–23 g) and 30 Sprague-Dawley (SD) rats (6–8 weeks old, weighing 250–300 g) were obtained from Hunan Slake Jingda Experimental Animal Co., Ltd. (Changsha, China). All animals were housed in accordance with standard protocols and acclimated for one week under controlled temperature and a 12-hour light/dark cycle prior to the start of the experiments. All surgeries were performed under isoflurane anesthesia, with efforts made to minimize animal suffering.

Medicine and Materials

CHQF (Z20220657000) was purchased from Hunan Dekang Pharmaceutical Co., Ltd (Hunan, China). L-arginine (A5006), cerulein (17650–98-5), lipopolysaccharide (LPS, 82857–67-8) were purchased from Sigma-Aldrich (Shanghai, China). IL-6 ELISA kit (EK206), IL-1β ELISA kit (EK201B), IL-18 ELISA kit (EK218), TNF-α ELISA kit (EK282HS) were purchased from Multi Sciences (Lianke) Biotech Co., Ltd (Wuhan, China). MPO detection kit (BC5710), CCK-8 Cell Proliferation and Cytotoxicity Assay Kit (CA1210) were purchased from the Beijing Solarbio Science & Technology Co., Ltd (Beijing, China). GAPDH rabbit mAb (R380626), NLRP3 rabbit mAb (381207), F4/80 rabbit mAb (263101), Goat Anti-Rabbit IgG H&L (AF488) (550,037), Goat Anti-Rabbit IgG H&L (Cy3) (550076) were purchased from Chengdu Zen Bioscience Co., Ltd (Chengdu, China). MMP9 rabbit mAb (ab38898) was purchased from the Abcam plc (Shanghai, China). Caspase-1 rabbit mAb (A0964) was purchased from the ABclonal Biotechnology Co., Ltd (Wuhan, China). ASC rabbit mAb (67824T) was purchased from the Cell Signaling Technology (Shanghai, China), GSDMD rabbit mAb (AF4012) was purchased from the Affinity Biosciences Co., Ltd (Liyang, China).

SAP Model Establishment and CHQF Intervention

All mice were randomly divided into five groups, each consisting of 30 mice: the control group (CON), the SAP group (SAP), the SAP + low-dose CHQF group (SAP + L-CHQF), the SAP + moderate-dose CHQF group (SAP + M-CHQF), and the SAP + high-does CHQF group (SAP + H-CHQF). In the SAP group, mice received two intraperitoneal (i.p.) injections of 8% L-arginine (4 g/kg, pH=7.0) with a 1-hour interval between two injections. In the control group, mice received normal saline (NS) injections. In the CHQF groups, prior to the L-arginine injection, mice received CHQF pretreatment (low dose: 0.68 g/kg; moderate dose: 1.35 g/kg; high dose: 2.7 g/kg) twice a day for 5 consecutive days.

Sample Collection and Preparation

12 hours after the second injection, the mice were anesthetized with 2% isoflurane. Blood samples were isolated, then centrifuged at 3000 rpm, with 300 μL of serum was collected, and stored at −80°C for further analysis. The pancreas and lung tissues were promptly dissected. One portion of the tissues were stored at −80°C for Western blotting or proteomics analysis, while the other portion was fixed in 4% paraformaldehyde solution for histological examination.

CHQF-Containing Serum Preparation

30 rats were randomly divided into two groups: the CHQF group (n=20) and the control group (n=10). Rats in the CHQF group received intragastric administration of CHQF (0.9 g/kg, twice a day for 7 consecutive days), while rats in the control group received an equivalent volume of distilled water. Two hours after the final gavage, rats were anesthetized with isoflurane, and serum samples were collected according to protocols mentioned above. After that, the serum was filtered through a 0.22 μm filter membrane, heat-inactivated at 56°C for 30 min, and stored at −80°C for further analysis.

Extraction of Metabolites From Serum

The serum (200 μL) were mixed with 20 μL hydrochloric acid solution (2 mol/L). The mixture was vortexed for 30s and sonicated for 5 min in a 4°C water bath. Next, 780 μL of acetonitrile was added to the sample, which was then vortexed for another 30s, sonicated for 5 min in the same 4°C water bath, and incubated for 30 min at −40°C to precipitate proteins. The samples were centrifuged at 12,000 rpm (RCF = 13,800 × g, R = 8.6 cm) for 15 min at 4°C. The final solutions were vortexed for 30s, sonicated for 1 min in 4°C water bath and centrifuged at 12,000 rpm (RCF = 13,800 × g, R= 8.6 cm) for 15 min at 4°C. The supernatant was then transferred to fresh glass vials for analysis. A quality control (QC) sample was prepared by mixing equal aliquots of the supernatant from each sample.

Extraction of Metabolites From CHQF

The CHQF powder (50 mg ± 2 mg) were taken and lyophilized. The powder was mixed with beads and 500 μL of extraction solution (MeOH:ACN:H$_2$O, 2:2:1 (v/v/v)) which contained deuterated internal standards. The mixture was vortexed for 30s, homogenized at 35 hz for 240s, and sonicated for 5 min in a 4°C water bath. The homogenization and sonication process was repeated 3 times. Then the mixed solution incubated for 30 min at −40°C to precipitate proteins. After incubation, the samples were centrifuged at 12,000 rpm (RCF = 13,800 × g, R = 8.6 cm) for 15 min at 4°C. The supernatant was transferred to fresh vials to incubate for 10 min and followed by another centrifugation at 12,000 rpm (RCF = 13,800 × g, R = 8.6 cm) for 15 min at 4°C. The new supernatant was then transferred to fresh glass vials for analysis. The QC sample was prepared by mixing an equal aliquot of the supernatant of samples.

LC-MS/MS Analysis

LC-MS/MS analyses were performed using an UHPLC system (Vanquish, Thermo Fisher Scientific, USA) with a Phenomenex Kinetex C18 (2.1 mm × 100 mm, 2.6 μm) coupled to an Orbitrap Exploris 120 mass spectrometer (Orbitrap MS, Thermo Fisher Scientific). The mobile phase A: 0.01% acetic acid in water; mobile phase B: IPA:ACN (1:1,v/v). The auto-sampler temperature was 4°C, and the injection volume was 2 μL. The Orbitrap Exploris 120 mass spectrometer was used for its ability to acquire MS/MS spectra on information-dependent acquisition (IDA) mode in the control of the acquisition software (Xcalibur, Thermo Fisher Scientific). In this mode, the acquisition software continuously evaluates the full scan MS spectrum. The ESI source conditions were set as following: sheath gas flow rate as 50 Arb, Aux gas flow rate as 15 Arb, capillary temperature 320°C, full MS resolution as 60,000, MS/MS resolution as 15,000, collision energy: SNCE 20/30/40, spray voltage as 3.8 kV (positive) or −3.4 kV (negative), respectively.

The raw data were converted to the mzXML format using ProteoWizard and processed with an in-house program, which was developed using R and based on XCMS, for peak detection, extraction, alignment, and integration. The R package and the BiotreeDB (V3.0) were applied in metabolite identification.

Proteomic Mass Spectrometric Analysis

The lung tissues were processed according to the Filter Aided Sample Preparation (FASP) method. Firstly, 300 μg total protein was added to 30 kDa molecular weight cutoff filters. The mixture was centrifuged at $10,000 \times g$ for 10 min (4°C). Wash the proteins with urea buffer for twice. IAA solution (50 mm) (100 μL) was added, and the mixture was incubated at room temperature for 30 min (protected from light). The mixture was centrifuged again and washed twice. After completion, appropriate trypsin was added to the column at a protein/trypsin ratio of 100:1. The sample was shaken at 37°C for 4 h. The same volume of trypsin was spiked into the sample and shaken at 37°C overnight before the elution ($10,000 \times g$ at room temperature). The column was washed with 50 mm NH_4HCO_3 (50 μL), and the eluate was combined. Peptide purification was conducted on a SOLA μ HRP column (60209–001, Thermo Fisher Scientific).

The peptides were loaded into an UltiMate 3000 Rapid Separation UHPLC Systems (Thermo Fisher Scientific) and analyzed by Orbitrap Exploris 240 mass spectrometer (BRE725535, Thermo Fisher Scientific). Firstly, the peptides were enriched through a trap column and separated using a C18 column (2 μm, Acclaim PepMap 100 C18 hPLC Columns, 100 Å, 250×0.075 mm) at a rate of 0.3 μL/min for 2.5 h, with the following gradient: 0–3 min: 3% B; 3–5 min: 3–5% B; 5–125 min: 5–40% B; 125–135 min: 40–95% B; 135–139 min: 95% B; 139–140 min: 95%-3% B; 140–150 min: 3% B. Buffer A consisted of HPLC water + 0.1% formic acid and buffer B contained 80% ACN + 0.1% formic acid + 20% HPLC water. The MS parameters were as follows: 2.15kV for the capillary voltage, 300°C for the capillary temperature and 7 units for the auxiliary gas flow. Peptides were analyzed in positive ionization modes with a scanning mass-to-charge (m/z) range from 350–1200 m/z at a resolution of 6000 with a maximum injection time of 20 ms and an AGC target value of 3e6. In addition, MS2 parameters were set as follows: Isolation windows was set to 10 m/z; resolution was set to 15,000; scanning mass-to-charge was set to 350–1200 m/z and normalized collision energy was set to 30%. Pierce FlexMix Calibration Solution used for mass and RT calibration were performed every three days. Blank sample (0.1% FA in HPLC water) was loaded every four samples.

Dataset Analysis From the GEO Database

The NCBI Gene Expression Omnibus (GEO) database (http://www.ncbi.nlm.nih.gov/geo) is an open genomic database that collects submitted high-throughput gene expression data. In this study, a comprehensive search of the GEO database was conducted for datasets related to AP research. Eligible studies included those that investigated pancreatic tissue or blood samples from AP patients, provided detailed information on the research techniques and platforms, and included a control group with normal samples. Adhering to these criteria, the GSE194331 dataset (platform file GPL16791), comprising 20 Moderately-severe AP (M-SAP) samples and 10 SAP samples (collectively defined as the SAP group) and 32 normal samples as the control group, was selected and downloaded on 10 May 2023.[13]

Identification and Visualization of (DEGs/DEPs)

Differentially expressed genes/proteins (DEGs/DEPs) identification were identified using the Limma package in the R software[14] based on the criteria of |logFC|>0.585 and adjusted p-value < 0.05. The identified DEGs/DEPs were then visualized using R packages (pheatmap, dplyr, ggplot2, ggrepel) to generate heatmaps and volcano plots.

Weighted Gene Co-Expression Network Analysis (WGCNA)

Initially, the R WGCNA package was employed to compute the correlation coefficients between gene pairs by Pearson's correlation coefficient to construct the gene co-expression matrix.[15] Following the principles of scale-free networks, a soft threshold (power = 2) was selected to establish a scale-free co-expression network, and the adjacency matrix was transformed into a topological overlap matrix. Hierarchical clustering was used to construct a dendrogram and identify gene modules, each containing a minimum of 200 genes. The correlation between the module's characteristic genes and the SAP phenotype was calculated, and the SAP-associated module was determined based on the highest correlation coefficient and smallest p-value. Core genes within the module were filtered by setting gene significance (GS) > 0.5 and module membership (MM) > 0.8.

Network Pharmacology Analysis

The blood-absorbed components of CHQF were screened using the criteria of oral bioavailability (OB ≥ 30%) and Drug-likeness (DL ≥ 0.18).[16] Subsequently, ChEMBL and DrugBank were used to search for targets associated with the components, and the target names were converted into the gene names via Uniprot. After that, integrated the gene names with SAP-related genes obtained from the GEO database. STRING v11.0b (https://string-db.org/) was used to construct Protein-Protein Interaction (PPI) network with a confidence score > 0.4. Cytoscape (version 3.10.1, Boston, MA, USA) was applied to construct the compound-target network.

Gene Function Enrichment Analysis

The R packages (clusterProfiler, enrichplot) were utilized to conduct Gene Ontology (GO) (http://geneontology.org/) and Kyoto Encyclopedia of Genes and Genomes (KEGG) (http://www.kegg.jp/ or http://www.genome.jp/kegg/) enrichment analyses. A p-value of less than 0.05 was considered significant.

Hematoxylin Eosin (H&E) Staining

The pancreas and lungs tissues fixed in 4% paraformaldehyde were used for H&E staining. First, the tissues were dehydrated, paraffin-embedded, and sectioned into 5μm-thick slices using a rotary microtome. H&E staining was then performed on the sections, followed by a series of steps including dehydration, clearing, and sealing. Tissue sections were examined and photographed using a microscope (ICC50 W, Leica Microsystems, Nussloch, Germany). Lung injury was assessed based on four aspects: interstitial inflammation, neutrophil infiltration, congestion, and edema. A grading system ranging from 0 to 4 was employed to describe the severity of tissue injury, where 0 represented minimal damage, 1 denoted mild damage, 2 indicated moderate damage, 3 signified severe damage, and 4 represented extremely severe damage. The lung injury score was calculated as the sum of individual scores from each category.

Lung Wet/Dry (W/D) Weight Ratio Measurement

Following the sacrifice of the mice, the entire lung was excised and immediately weighted to obtain the wet weight (W). Subsequently, the wet lung tissue was placed in an oven at 60°C for 48 hours and reweighted to determine the dry weight (D). The W/D ratio was then calculated by dividing the wet weight by the dry weight.

Determination of Myeloperoxidase (MPO) Activity

MPO activity was detected according to the manufacturer's instructions for the MPO detection kit. 12 hours after the second injection, lung tissues were collected and homogenized in an ice bath, followed by centrifugation at 12,000g for 10 min at 4°C. The samples were then added to a 96-well plate, and optical density (OD) values were measured at a wavelength of 460 nm using a spectrophotometer (Multiskan™ FC 51119080, Thermo Scientific).

Enzyme-Linked Immunosorbent Assay (ELISA)

IL-6, IL-1β, IL-18, and TNF-α levels in the serum and cell culture supernatant were measured using an ELISA kit according to the manufacturer's instructions.

Pancreatic Acinar Cells-Alveolar Macrophages Co-Culture

Pancreatic acinar cells (266–6 cell line) were co-cultured with alveolar macrophages (MH-S cell line) in 6-well Tissue Culture Plate Inserts (TCS-018-006, JET BIOFIL, Guangzhou, China) in an environment of 5% CO_2 and 37 °C in CHQF-containing sera supplemented with cerulein (100 nmol/L) and LPS (10 μg/mL).[17] As controls, 266–6 cells were co-cultured with MH-S cells in basic culture medium containing 10% normal rat-derived sera. After 12 hours, MH-S cells were collected for Western blot analysis, and the corresponding culture medium was utilized for further detection.

Western Blot Analysis

Lung tissue or MH-S cells were lysed in radioimmunoprecipitation (RIPA) assay buffer containing a protease inhibitor cocktail. Protein concentration was determined using BCA assay. The lysates were then mixed with SDS protein loading

buffer and boiled in preparation for electrophoresis. Total protein (30 μg) was separated by 8–12% SDS-PAGE and subsequently transferred onto PVDF membranes. The membranes were blocked with 5% non-fat milk at room temperature for 1 hour, followed by overnight incubation at 4°C with primary antibodies. The antibodies used included: anti-GAPDH (1:1000), anti-MMP9 (1:1000), anti-ASC (1:1000), anti-NLRP3 (1:1000), anti-GSDMD (1:1000), and anti-Caspase-1 (1:1000). After primary antibody incubation, the membranes were washed three times with TBST and then incubated with the corresponding secondary antibodies (1:1000) at room temperature for 1 hour, followed by three additional TBST washes. Specific bands were visualized using the ECL chemiluminescence kit and detected with the gel imaging system (Omega Lum™ C, Bio-rad, California, USA). Protein band intensities were measured and quantified using Image J software.

Multichannel Immunofluorescence Staining

Murine lungs were dissected in ice-cold PBS buffer and fixed in 4% paraformaldehyde. Multichannel immunofluorescence staining was performed directly on slides containing 20 μm sections. After incubating the slices in a blocking buffer for 1 hour, they were subjected to overnight incubation with the anti-F4/80 antibody at 4 °C. The slices were then washed three times and incubated with the secondary antibody in the dark at room temperature for 1.5 hours. Following this, the slices were re-blocked, and a combination of anti-NLRP3, anti-Caspase-1, anti-MMP9 and anti-ASC antibodies, along with their respective secondary antibodies, was added. Finally, the nuclear stain DAPI was added during the final wash and imaged using fluorescence microscopy (Pannoramic SCAN II, 3DHISTECH, Budapest, Hungary).

Immunofluorescence

MH-S cells were resuspended in 1 mL PBS, and 40 μL of the cell suspension was dropped onto poly-D-lysine-coated glass coverslips. The cells were then fixed with 4% paraformaldehyde for 10 min. For tissues, the lung tissue was dehydrated, embedded in paraffin wax, and cut into 5 μm sections. The sections were deparaffinized, and antigen retrieval was performed using EDTA antigen retrieval solution. After this, the glass coverslips or sections were blocked with 3% goat serum for 30 min, followed by incubation with the primary antibodies (1:200) at 4°C overnight. Subsequently, the samples were incubated with the corresponding secondary antibodies (1:200) at room temperature for 1 hour. The cells and tissues were visualized using fluorescence microscopy (DM2500, Leica Microsystems).

Statistical Analysis

Statistical analysis was conducted using GraphPad Prism 9.0 software or R language. All data were presented as mean ± SEM (standard error of the mean), with each experiment repeated independently at least three times. The Student's t-test was used to compare two groups for normally distributed data, while the the Mann–Whitney U-test were employed for non-normally distributed data. The chi-square test was used to analyze categorical data between two groups. For multiple comparisons, one-way analysis of variance (ANOVA) with Bonferroni correction was used when the assumption of homogeneity of variance was met. If the assumption was violated, the Kruskal–Wallis test was applied. The Mantel-Cox Log rank test was performed to compare survival curves. Correlation was assessed by the Spearman rank correlation test. Statistical significance was defined as $p < 0.05$.

Results

CHQF Significantly Reduces the Incidence of ALI in AP Patients

In order to investigate the potential preventive and therapeutic effects of CHQF on AP-ALI, a retrospective analysis of the clinical characteristics of 92 AP patients was conducted (Table 1). Patients were stratified into two groups based on whether they received CHQF after diagnosis. Among the AP patients, no significant differences were observed in the baseline characteristics, including gender, age, etiology, and baseline APACHE II, Balthazar CT, and BISAP scores within the 24 hours prior to treatment initiation. However, the incidence of ALI was reduced by 21.97%, and the average duration of invasive mechanical ventilation decreased from 13.5 ± 2.14 days to 5.33 ± 1.86 days in the CHQF-treated group compared to the control group. These findings suggest that CHQF may reduce the incidence of ALI in AP patients.

2323

Table 1 Baseline Characteristics and Primary Outcomes in the Two Groups

	Control group (n = 48)	CHQF group (n = 44)	t/U/χ^2	P value
Baseline Clinical Data				
Gender			0	0.98
Male	37(77.08%)	34(77.27%)		
Female	11(22.92%)	10(22.73%)		
Age (years)	41.88±1.43	43.64±2.16	0.68	0.49
Etiological factor			1.96	0.38
Biliary tract stone	5(10.42%)	9(20.45%)		
Hyperlipidemia	41(85.42%)	34(77.27%)		
Alcohol intake	2(4.17%)	1(2.27%)		
Other	0	0		
APACHE II score	4.65±0.66	5.97±0.81	853.5	0.11
Balthazar CT score	2.41±0.32	2.73±0.36	985	0.57
BISAP score	1.40±0.13	1.18±0.14	912	0.23
Primary outcomes				
ICU admission	20(41.67%)	19(43.18%)	0.02	0.88
Hospital stay (days)	8.77±0.71	10.84±1.09	907	0.24
ALI	28(58.33%)	16(36.36%)	4.44	0.04
Mechanical ventilation	6(12.5%)	3(6.82%)	0.84	0.36
Duration of mechanical ventilation (days)	13.5±2.14	5.33±1.86	1	0.048
In-hospital mortality	4(8.3%)	2(4.5%)	0.54	0.46

CHQF Alleviates ALI in SAP Mice Induced by L-Arginine

To investigate the protective effects of CHQF on SAP, we established an SAP mouse model using L-arginine and treated the mice with CHQF prior to L-arginine injection. The protective effects of CHQF were evaluated by assessing survival rate, pathological changes, inflammatory mediators, and biochemical markers in the serum. As shown in Figure 1A, the survival rate decreased from 100% to 40% after 72 hours of L-arginine injection, which can be increased after the gavage administration of CHQF (Figure 1A). Additionally, CHQF pretreatment significantly alleviated hepatic and renal function impairment in SAP mice (Figure 1B-E), and lowered the levels of serum inflammatory factors IL-6 and TNF-α (Figure 1F-G). What's more, the MPO and W/D ratio detection of lung tissues showed a similar protective effect (Figure 1H-I). Pathological investigation revealed that CHQF administration significantly reduced pancreatic necrosis and inflammatory cell infiltration, and lowered the pathological damage score in lung tissues (Figure 1J-K).

A middle dose of CHQF was selected for subsequent experiments due to its observed protective effects and suitability for gavage administration. This selection was based on a comprehensive evaluation of dose effects and experimental objectives, ensuring the reliability, consistency, and reproducibility of the results in future studies.

Screening of SAP-Related DEGs

To further investigate the potential molecular mechanisms underlying SAP, we performed a secondary analysis of the GSE194331 dataset, which contains 30 SAP samples and 32 healthy samples. First, we screened for DEGs by applying the criteria of |logFC| > 0.585 and adjusted $p < 0.05$, resulting in a total of 4925 DEGs, including 2222 upregulated and 2703 downregulated genes (Figure 2A). A heatmap of top 50 upregulated and downregulated genes is diagrammed in Figure 2B. Next, to precisely identify key genes associated with the SAP phenotype, we employed the WGCNA algorithm to construct a gene co-expression network. A soft threshold of 2 was applied to achieve an approximately scale-free topology with a corresponding $R^2 > 0.8$ (Figure 2C). A gene hierarchical clustering dendrogram was then generated based on gene correlations, yielding 49 distinct gene modules (Figure 2D). Among these, the "blue" module, comprising 19,312 genes, was identified as the most clinically relevant to SAP based on its strong correlation with the SAP phenotype (Cor = 0.8, $p = 6e−15$) (Figure 2E). The scatter plot
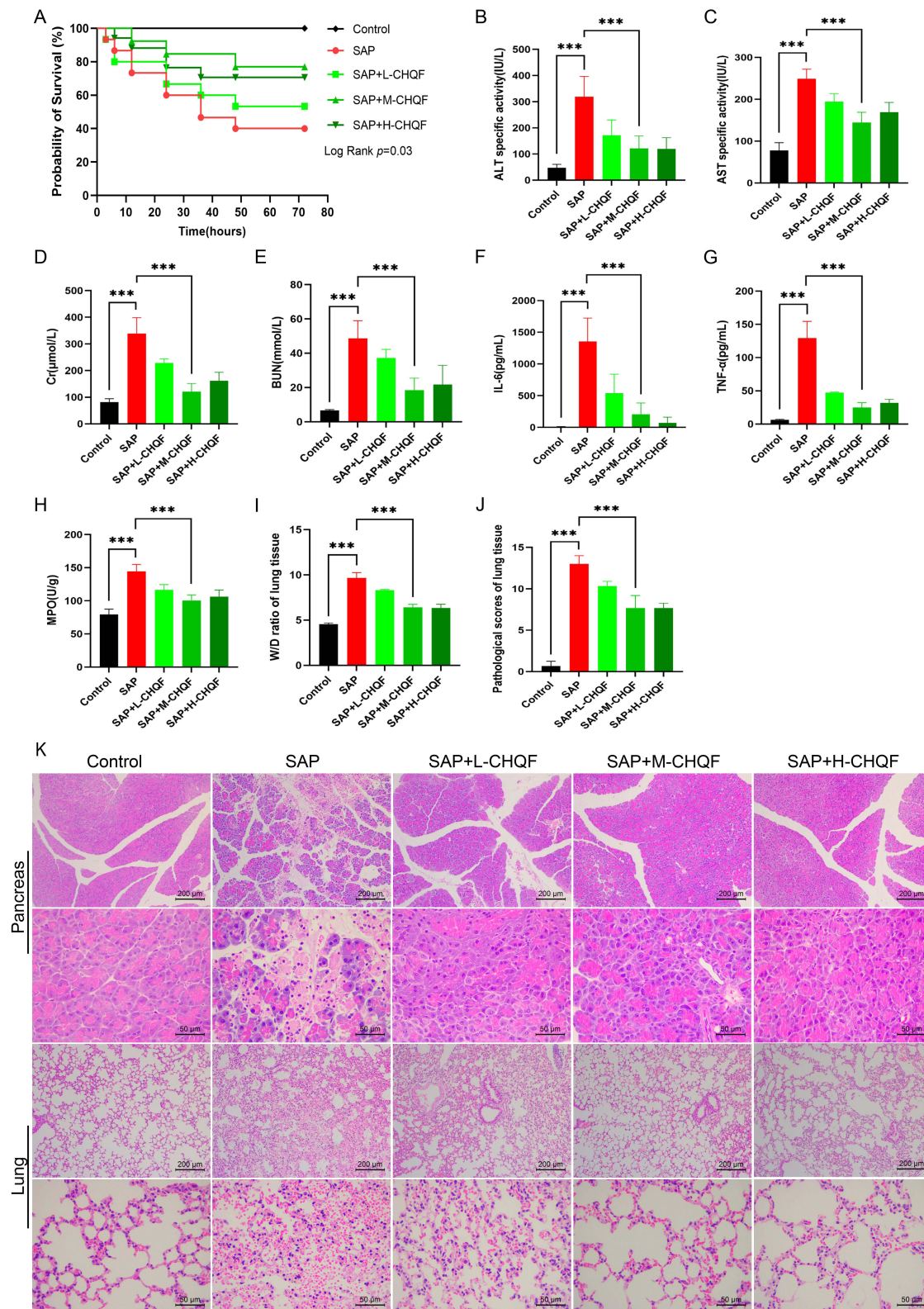
Figure 1 Protective effects of CHQF on SAP mice. (**A**) The survival curves of mice in each group (n=15). (**B-E**) Detection for the liver and kidney function indexes (n=5). (**F, G**) Detection for IL-6 and TNF-α levels (n=5). (**H**) The MPO levels in lung tissues (n=5). (**I**) The lung W/D ratio (n=3). (**J-K**) H&E staining of the pancreas (upper) and lung tissues (lower) (n=3). ***P<0.001.
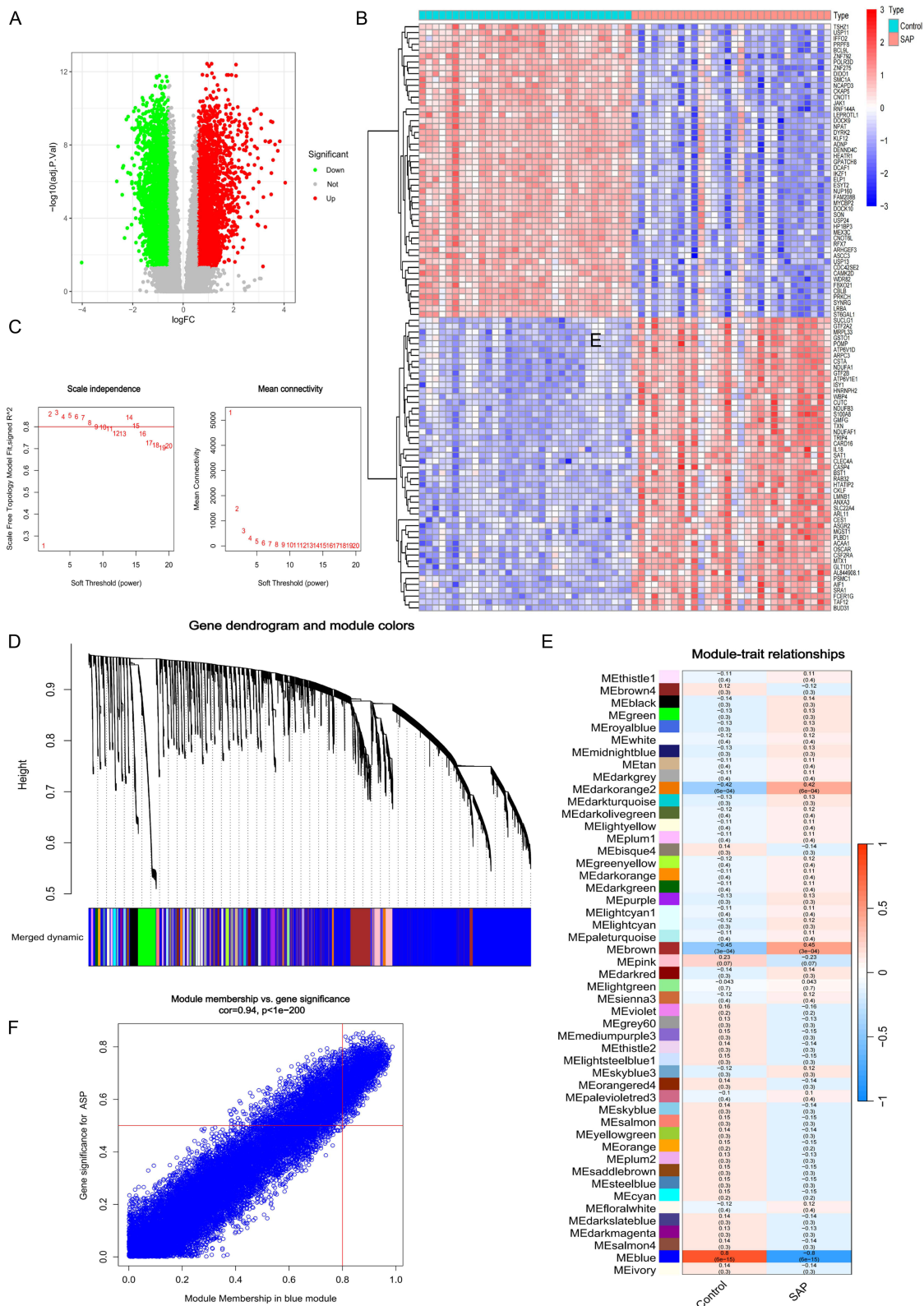
Figure 2 Screening of SAP-related DEGs. (**A**) Volcano plot of DEGs in SAP patients and healthy controls. (**B**) Heatmap of the top 50 upregulated and downregulated genes. (**C**) The scale plot of WGCNA to identify optimal vector power (cutoff value = 0.8). (**D**) Sample dendrogram and trait heatmap. (**E**) The module correlation heatmap: every module has its correlation coefficient and corresponding *p*-value. (**F**) The blue module's GS and MM values.

([Figure 2F](#)) illustrated a robust correlation (Cor = 0.94, $p < 1e{-}200$) between Gene Significance (GS) and Module Membership (MM) within the "blue" module.

Potential Therapeutic Targets for CHQF in the Treatment of SAP

To explore the potential material basis of CHQF in treating SAP, we performed serum pharmacochemical analysis of its components using an LC-MS/MS quadrupole-Orbitrap mass spectrometer system in both positive and negative ion modes ([Figure 3A-B](#)). A total of 172 compounds absorbed into the blood were identified. These compounds were filtered based on criteria of OB $\geq$ 30% and DL $\geq$ 0.18, resulting in the selection of 26 compounds and the identification of 271 associated therapeutic targets ([Supplementary Table 1](#)).

To investigate the potential targets of CHQF in treating SAP, we performed an integrated analysis of 4925 DEGs, 19,312 SAP clinical-associated genes, and CHQF-associated targets, leading to the identification of 52 overlapping targets ([Figure 4A](#)). A protein-protein interaction (PPI) network of these intersecting targets was then constructed using
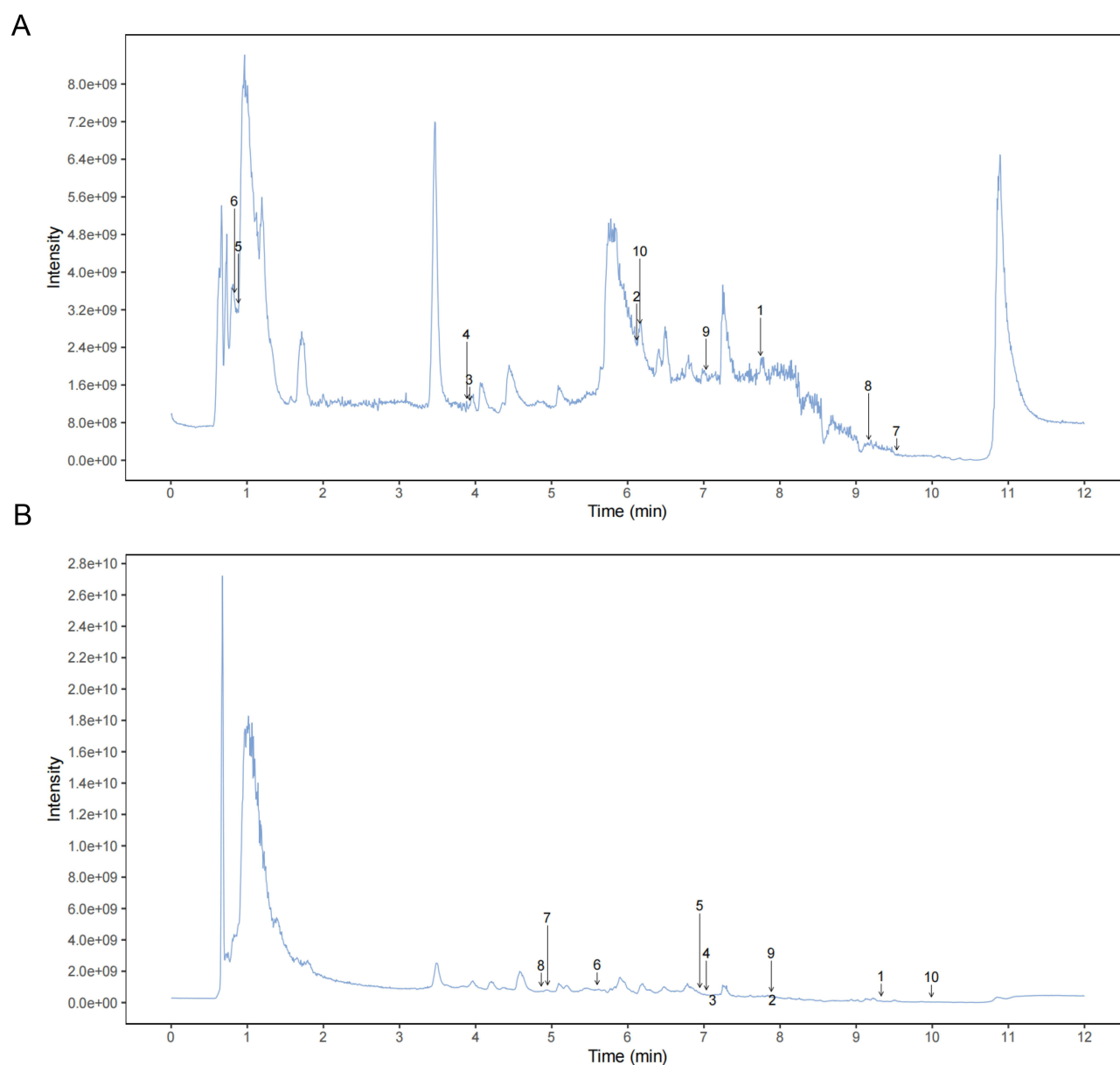
Figure 3 Ion flow diagram of UHPLC-MS/MS. (**A**) Positive ion mode. (**B**) Negative ion mode.
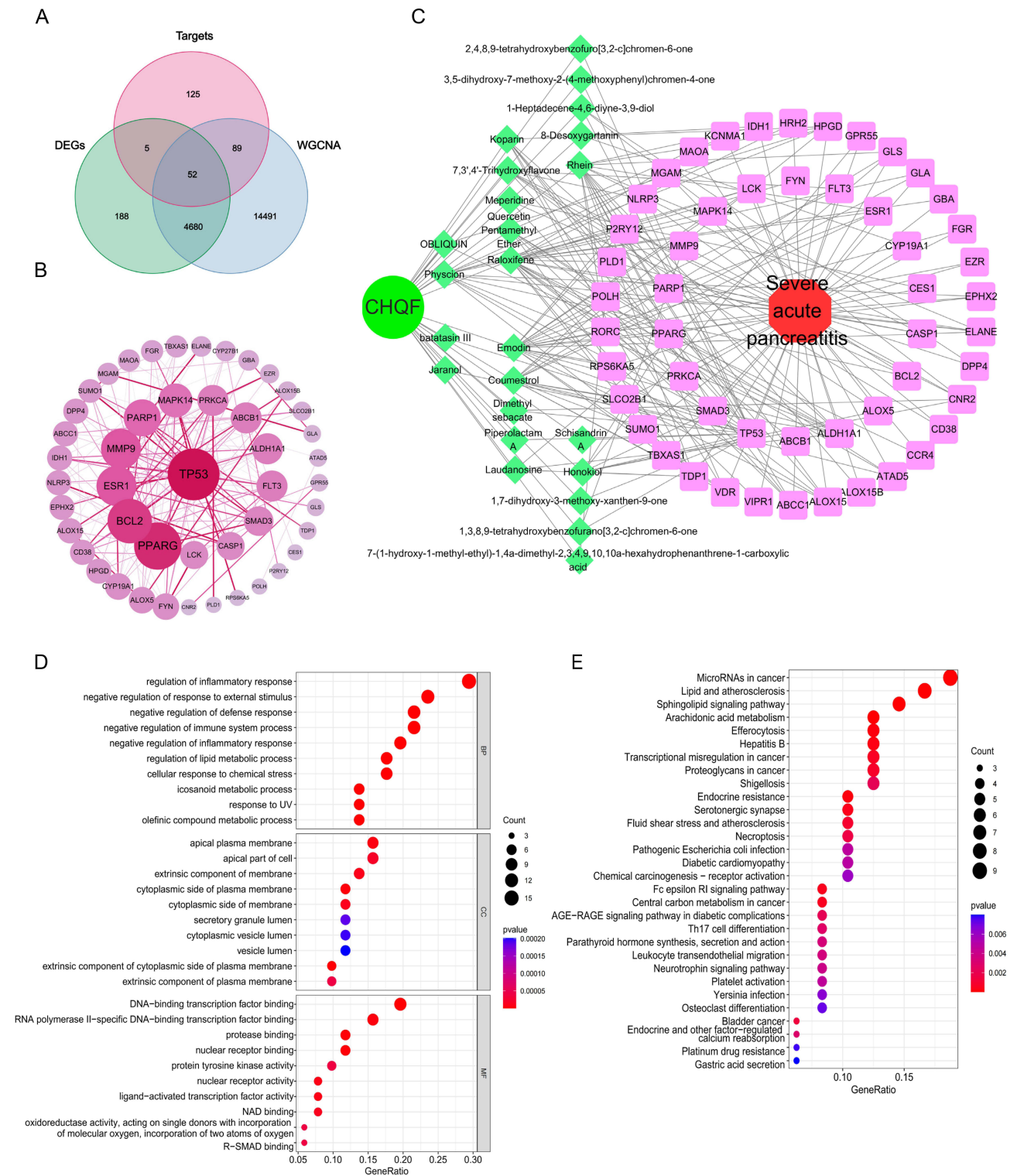
Figure 4 Potential therapeutic targets for CHQF in treating SAP. (**A**) Venn diagram of the overlapping genes among DEGs, blue module genes, and CHQF associated targets. (**B**) PPI network of the intersection targets. The shade of purple is directly proportional to the degree value. (**C**) Network of CHQF absorbed components and associated targets, diamonds representing the components and squares representing the potential targets. (**D**) GO enriched analysis. (**E**) KEGG pathway analysis.

STRING, followed by key target identification through Cytoscape. The critical targets identified included TP53, PPARG, BCL2, ESR1, MMP9, PARP1, among others (Figure 4B). Additionally, a regulatory network connecting CHQF components to the overlapping targets was constructed using Cytoscape, with diamonds representing the components and squares representing the potential targets (Figure 4C).

GO enrichment analysis of the overlapping targets revealed 1,228 enriched pathways, including 121 terms in molecular functions (MF), 50 in cellular components (CC), and 1057 in biological processes (BP). Among these pathways, regulation of inflammatory response, response to oxidative stress, protein binding, and leukocyte migration were highly enriched (Figure 4D). KEGG enrichment analysis identified 66 significant pathways, primarily involving arachidonic acid metabolism, the IL-17 signaling pathway, necroptosis, and platelet activation, among others (Figure 4E).

Quantitative Proteomic Analyses of SAP-ALI Lung Tissue

Changes in protein levels serve as a primary indicator of cellular functional alterations. To precisely assess the effects of CHQF on SAP-associated ALI, we conducted proteomic analysis to evaluate differential protein expression in the lung tissues of SAP mice treated with or without CHQF. A total of 1234 DEPs were identified between the control and SAP groups, including 406 upregulated proteins and 828 downregulated proteins (Figure 5A). Additionally, CHQF treatment resulted in alterations in 582 proteins compared to the SAP group, including 165 upregulated and 417 downregulated proteins (Figure 5B). The Venn diagram shows the overlapping DEPs among the three groups (Figure 5C), and the detailed data of these overlapping DEPs can be found in Supplementary Table 2. Furthermore, a heatmap presents the top 50 overlapping DEPs exhibiting the most significant differential expression between the SAP and control groups (Figure 5D).
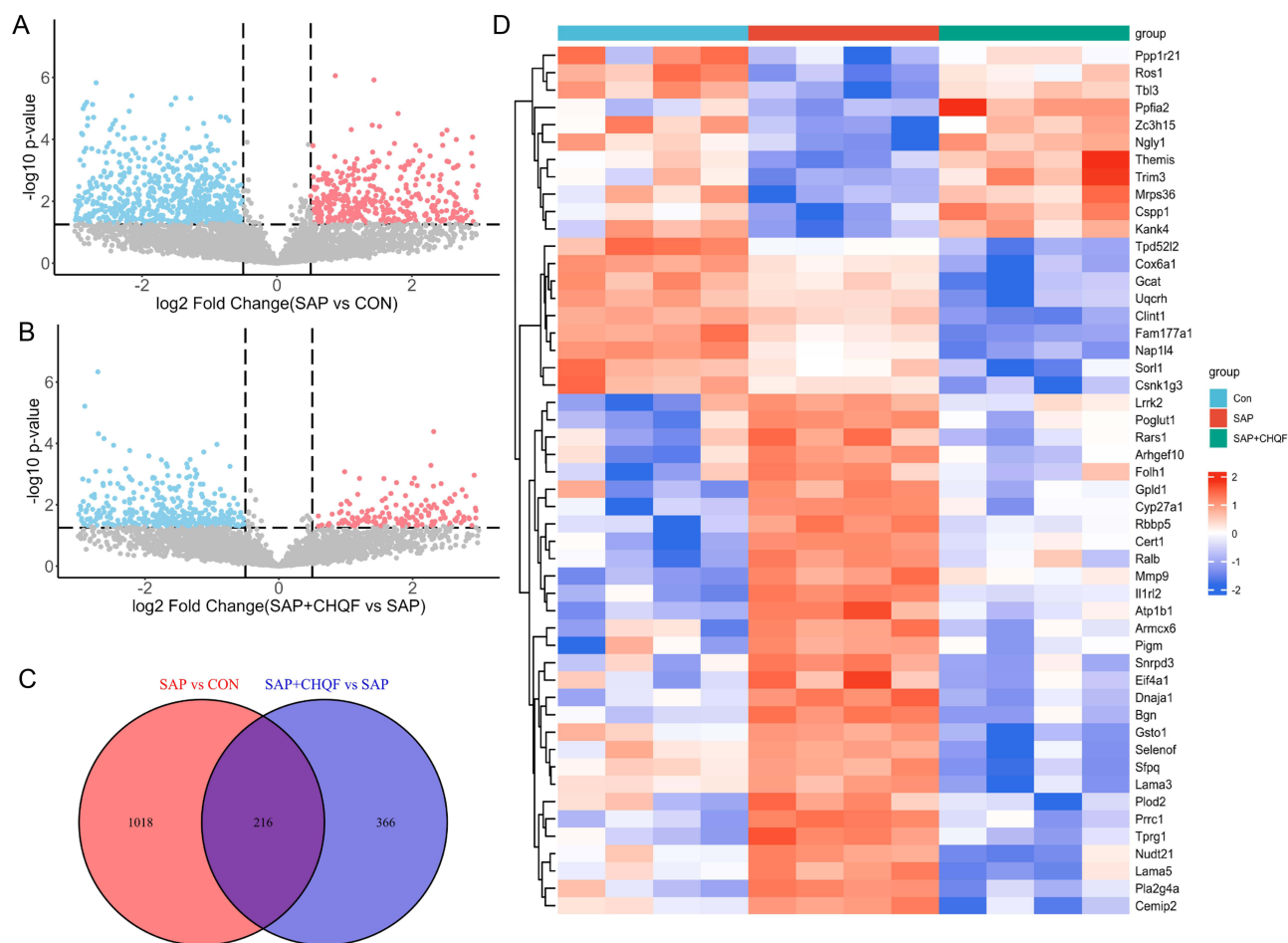

Figure 5 Quantitative proteomic analysis of mouse lung tissue in SAP-ALI. (**A, B**) Volcano plot of DEPs. (**C**) Venn diagram of the DEPs. (**D**) Heatmap of the top 50 DEPs.

MMP9 and NLRP3 are the Key Targets of CHQF in Alleviating SAP-ALI

To identify the crucial targets, a joint analysis of DEPs and CHQF/SAP-associated targets was conducted. As a result, MMP9 and NLRP3 were identified as key targets for CHQF in treating SAP-ALI (Figure 6A). Numerous studies have demonstrated a correlation between MMP9, NLRP3, and pyroptosis.[18–21] In this study, we further analyzed pyroptosis-related molecules at the RNA level using the GSE194331 dataset, revealing a significant elevation of MMP9, NLRP3, and pyroptosis-related genes in the SAP group compared to the control group (Figure 6B-I). Our experimental data confirmed similar findings at the protein level (Figure 6J-L). However, CHQF administration reduced serum levels of IL-1β and IL-18 (Figure 6J-K), as well as the protein expression levels of MMP9, NLRP3, ASC, GSDMD-N, and Caspase-1 in lung tissues (Figure 6L). These findings suggest that CHQF's protective role in treating SAP-ALI may be attributed to its modulation of MMP9, NLRP3, and pyroptosis-associated proteins.

CHQF Attenuates Macrophage Pyroptosis in SAP-ALI

Macrophages, a major type of immune cell in the lung, play a crucial role in clearing invading pathogens through the release of inflammatory cytokines, a process in which NLRP3 is critically involved and can lead to pyroptosis.[22] Futhermore, MMP9 is primarily released by the macrophages, and can be rapidly activated in response to external stimuli.[19,23] To investigate the correlation between MMP9, NLRP3 and AMs in SAP-ALI, we examined the expression of MMP9 and NLRP3 and assessed pyroptosis in AMs through multichannel immunofluorescence staining. As shown in Figure 7A, the MMP9 and NLRP3 expression levels were significantly elevated in SAP lung tissues compared to the control group, with strong co-localization of these proteins observed in AMs. Notably, these effects were reversed by CHQF treatment. Furthermore, AMs in the SAP group exhibited more pronounced pyroptosis compared to the control group, which was also attenuated following CHQF administration (Figure 7B-C). These findings suggest that CHQF treatment reduces MMP9 expression and alleviates NLRP3-mediated pyroptosis in AMs.

CHQF Attenuates Macrophage Pyroptosis in Vitro

We next co-cultured pancreatic acinar cells and MH-S cells to validate our findings. First, the effect of CHQF-containing serum at different concentrations on MH-S proliferation was evaluated by the CCK8 assay (Figure 8A). Then, we simulated SAP-induced conditions in vitro to investigate the influence of CHQF-containing serum on MMP9 levels and pyroptosis in AMs. The ELISA results of cell culture medium showed a significantly elevation in IL-1β and IL-18 levels after stimulation with caerulein and LPS and these findings can be attenuated by treatment with CHQF-containing serum (Figure 8B-C). Western blot results showed a significant increase in MMP9 expression in AMs after stimulation with caerulein and LPS, along with pronounced pyroptosis, as evidenced by elevated levels of NLRP3, ASC, GSDMD, and Caspase-1. These effects were mitigated by treatment with CHQF-containing serum (Figure 8D). Our immunofluorescence assay also yielded similar results for the detection of the pyroptosis marker protein GSDMD (Figure 8E).

CHQF Attenuates Macrophage Pyroptosis Through the MMP9-NLRP3 Pathway

Our previous experiments demonstrated that MMP9 and NLRP3 are closely linked in AMs during SAP. To further investigate the relationship between MMP9 and NLRP3-related pyroptosis in SAP, we used the specific MMP9 inhibitor, MMP9-IN-1, in an in vitro co-culture system to simulate its effects on AMs under SAP stimulation. The results showed that MMP9-IN-1 significantly reduced caerulein + LPS induced NLRP3-mediated pyroptosis in AMs (Figure 9A-D), confirming that MMP9 contributes to the activation of the NLRP3 inflammasome, which drives the pyroptotic response. These findings suggest that the protective effect of CHQF in SAP-ALI may be related to its modulation of the MMP9-NLRP3-macrophage pyroptosis pathway.

Discussion

Lung injury is one of the most critical complications of AP, and widely recognized therapeutic interventions are still lacking.[24–27] In recent decades, TCM has attracted increasing attention for its unique advantages in anti-inflammatory and immunomodulatory activities, as well as its ability to regulate multiple physiological systems,[6,28,29] making it a promising avenue for the treatment of SAP-ALI. Our clinical data and animal experiments showed that CHQF is highly effective in
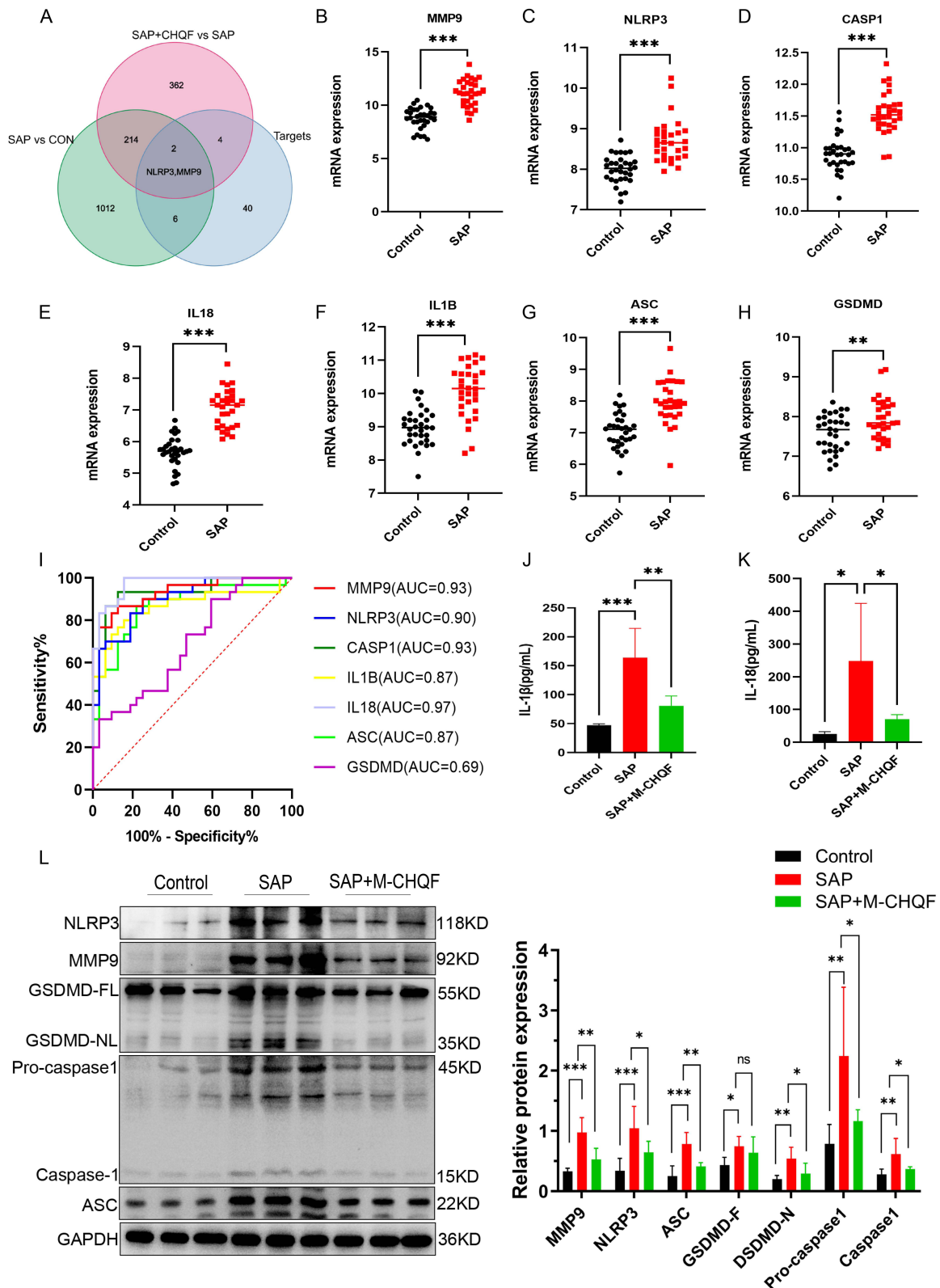
Figure 6 MMP9 and NLRP3 are key targets of CHQF in treating SAP-ALI. (**A**) Venn diagram showing the overlap between DEPs and CHQF/SAP-associated targets. (**B-H**) Expression levels of MMP9, NLRP3 and pyroptosis-related genes in SAP patients compared to healthy controls. (**I**) ROC analysis of MMP9, NLRP3, and pyroptosis-related genes. (**J-K**) Serum levels of IL-1β (n=5) and IL-18 (n=5). (**L**) Western blot analysis of the protein expression levels of MMP9, NLRP3, ASC, GSDMD-N, and Caspase-1 in lung tissues (n=3). ns: not significant, *P<0.05, **P<0.01, ***P<0.001.
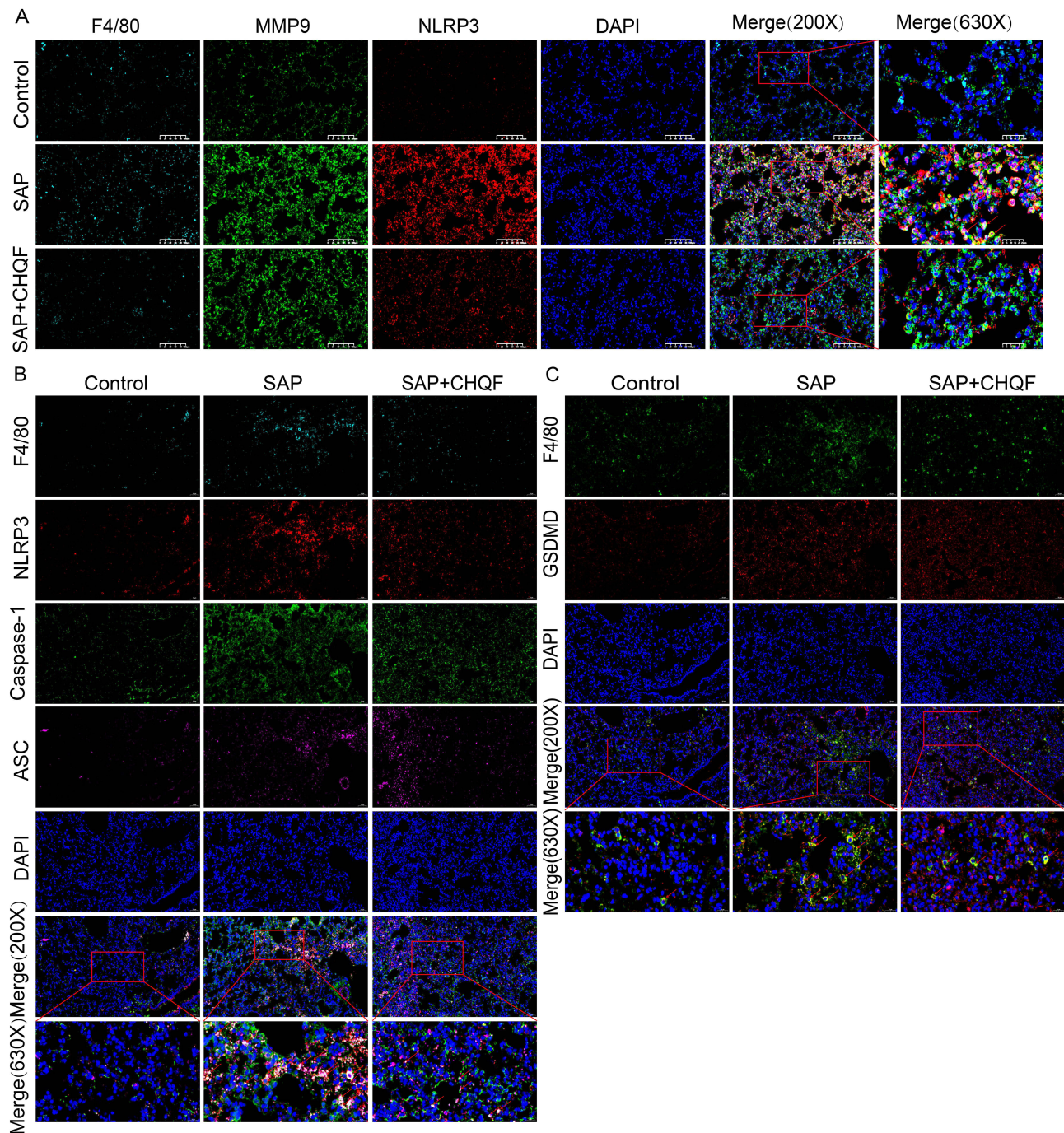
Figure 7 CHQF treatment reduces the expression of MMP9 and alleviates NLRP3-driven pyroptosis in AMs. (**A**) Multichannel immunofluorescence staining of MMP9, NLRP3 in AMs (n=3). (**B**) Multichannel immunofluorescence staining of NLRP3, Caspase-1, and ASC in AMs (n=3). (**C**) Multichannel immunofluorescence staining of GSDMD in AMs (n=3).

reducing the incidence of SAP-ALI, alleviating organ injury, and mitigating inflammation. These findings suggest that CHQF plays a protective role in the progression of SAP-ALI and may contribute to improving patient outcomes.

CHQF is derived from the well-known formula Qingyi Decoction, which has long been used in clinical practice to treat SAP due to its anti-inflammatory, antioxidant, anti-cell death and immunomodulatory properties.[6,10,30,31] Compared to Qingyi Decoction, CHQF, with the dosage changed from decoction to pill, is much more suitable for clinical application due to its convenient administration and precise dosage control. In this study, we comprehensively
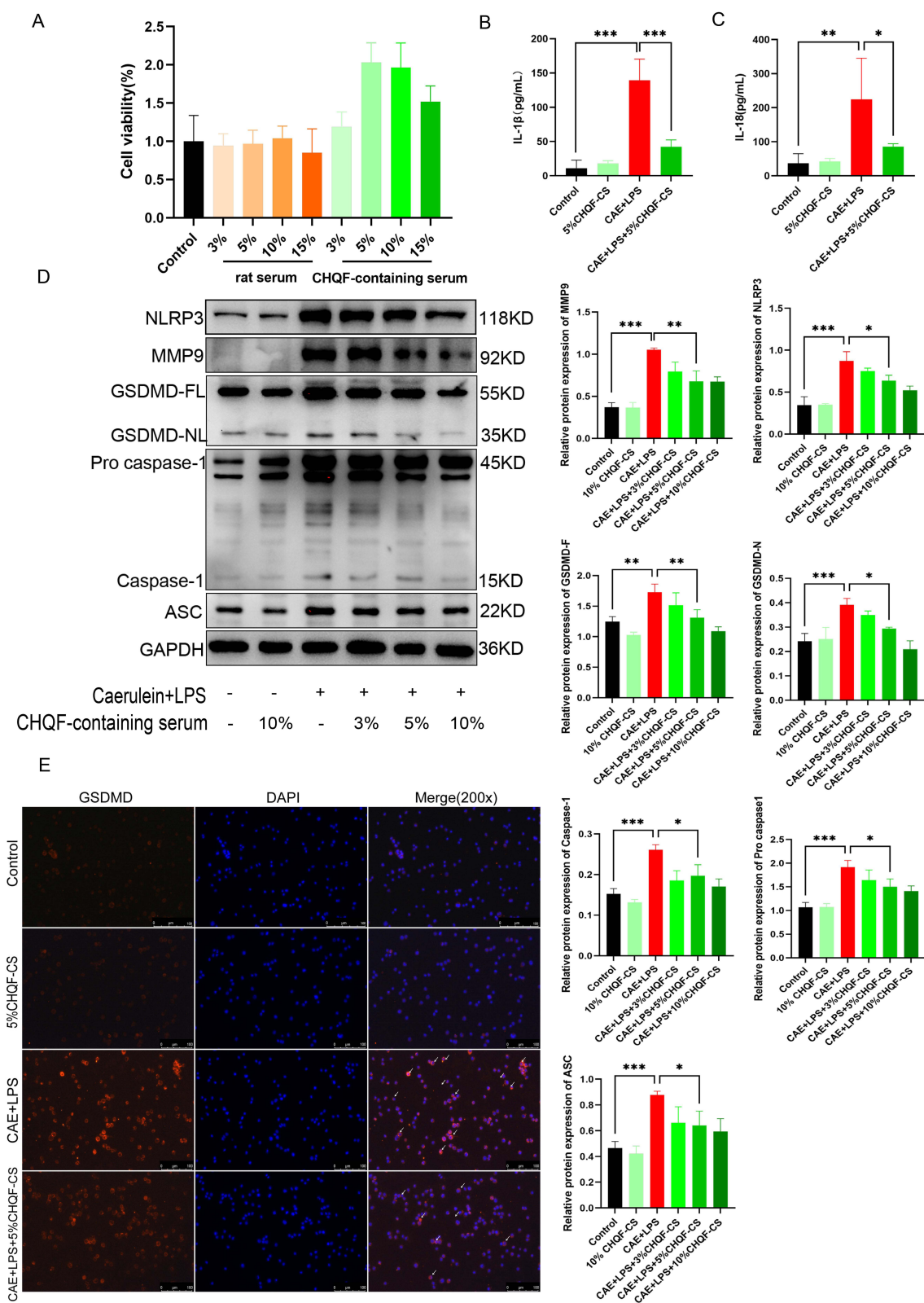
Figure 8 CHQF-containing serum attenuates AMs pyroptosis in vitro. (**A**) CCK8 assay for cell proliferation (n=5). (**B,C**) IL-1β and IL-18 levels in the culture medium (n=5). (**D**) Western blot analysis showing the expression levels of MMP9, NLRP3, and pyroptosis-related proteins in MH-S cells (n=3). (**E**) Immunofluorescence assay showing GSDMD levels in MH-S cells (n=3). *P<0.05, **P<0.01,***P<0.001.
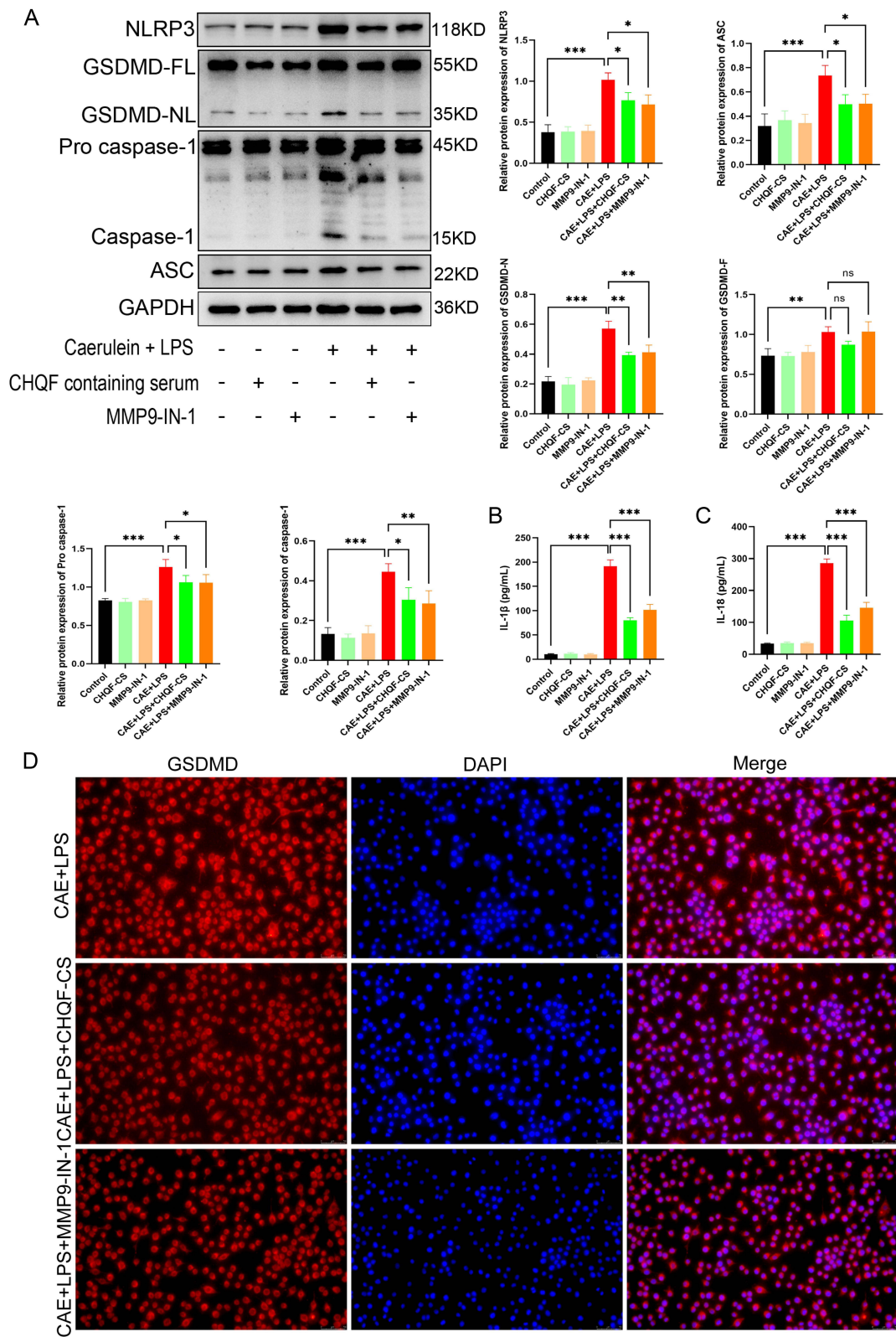
Figure 9 CHQF attenuates AMs pyroptosis through the MMP9-NLRP3 pathway. (**A**) Western blot analysis showing the expression levels of NLRP3 and pyroptosis-related proteins in MH-S cells (n=3). (**B,C**) IL-1β and IL-18 levels in culture medium (n=5). (**D**) Immunofluorescence assay showing GSDMD levels in MH-S cells (n=3). ns: not significant, *P<0.05, **P<0.01,***P<0.001.

investigated the therapeutic effects and molecular mechanisms of CHQF in treating SAP-ALI for the first time. We screened out the SAP-related core DEGs from the GSE194331 dataset, which revealed pathways and factors involved in the progression of SAP at the RNA level. Given the advantages of multiple components, multiple targets and multiple pathways observed in Chinese Medicine, we innovatively constructed a network to explore the complex associations among diseases, components absorbed into the blood, and their therapeutic targets. Our data identified 52 potential targets for CHQF in treating SAP. These findings highlighted significant enrichment in pathways related to inflammation, oxidative stress, necroptosis and cell apoptosis, which are the key contributors to the pathogenesis of SAP.[32–34] Considering the high incidence of ALI in SAP, we next focused on elucidating the specific mechanisms by which CHQF treats SAP-ALI. Therefore, proteomics analyses of the lung tissues was performed. After a joint analysis among the transcriptomics, network pharmacology and proteomics, we specifically identified MMP9 and NLRP3 as the only common targets.

NLRP3 is a crucial inducer of pyroptosis, as it can assemble a cytosolic innate immune complex that activates the cysteine protease caspase-1, which in turn cleaves gasdermin D (GSDMD) to trigger pyroptosis.[35] The important role of pyroptosis, especially macrophage pyroptosis, in inflammation-related ALI is well-documented.[22,36,37] Our results showed CHQF significantly inhibits NLRP3-induced pyroptosis in AMs of SAP mice, providing strong theoretical support for the clinical application of CHQF in the prevention and treatment of SAP-ALI. MMP9 is a gelatinase expressed by leukocytes, fibroblasts, epithelial, and endothelial cells, whose role in inflammatory cell migration, extracellular matrix degradation, and macrophage polarization has been well established.[38–42] Several studies have observed that its levels are elevated early in SAP, correlating with pulmonary complications.[43,44] However, the relationship between MMP9 and AMs pyroptosis remains poorly understood. Our study confirmed an association between MMP9 and NLRP3 in AMs. Current research suggests that both MMP9 and NLRP3 are regulated by NF-κB signaling,[45] and some studies propose that NLRP3 acts as an upstream regulator of MMP9.[21,46] However, in this study, we found that targeted inhibition of MMP9 can regulate NLRP3 expression and influence AMs pyroptosis, providing evidence of a positive feedback loop between MMP9 and NLRP3 in AMs during SAP-ALI. The mutual promotion of expression and activation of MMP9 and NLRP3 ultimately leads to an inflammatory cascade. Furthermore, the blood-absorbed components of CHQF effectively disrupt this feedback loop, exerting a protective effect against SAP-ALI. Based on the above results, our study provides a solid foundation for the clinical application of CHQF, which holds promise as a potential alternative to Qingyi Decoction in clinical practice.

There are still some limitations in our study. Firstly, our clinical findings are solely based on a small-sample retrospective study, and the relevant conclusions necessitate further confirmation in large-scale prospective studies. Secondly, the effect of CHQF on AMs pyroptosis has yet to be verified in human experiments. Moreover, although our study identified the relationship between MMP9 and NLRP3-driven pyroptosis in SAP-ALI, the underlying mechanisms remain unclear. The interaction between MMP9 and NLRP3 in AMs may involve multiple pathways. Our immunofluorescence results suggest co-localization of the two proteins in AMs, indicating a potential direct interaction, which is consistent with the findings of Fan et al in vascular smooth muscle cells.[47] Additionally, some studies in cardiac stem cells suggest that MMP9 regulates NLRP3 through an ROS-mediated pathway.[20] The precise relationship between these two in SAP mouse AMs requires further investigation.

Conclusion

In conclusion, this study is the first to explore the therapeutic effects and mechanisms of CHQF in treating SAP-ALI through an integrated multi-omics approach, combining transcriptomics, proteomics, serum pharmacochemistry and network pharmacology across clinical, animal, and cellular levels. We demonstrated that CHQF exerts its protective effects by modulating the MMP9-NLRP3 pathway, thereby alleviating AMs pyroptosis and mitigating SAP-ALI. Our findings provide novel insights into the pathogenesis of SAP-ALI and highlight the potential of CHQF for clinical application in the treatment and management of SAP-ALI.

Abbreviations

CHQF, Chaihuang Qingfu Pills; SAP, Severe acute pancreatitis; ALI, Acute lung injury; WGCNA, Weighted Gene Co-expression Network Analysis; DEGs/GEPs, Differentially Expressed Genes/proteins; TCM, Traditional Chinese medicine; APACHE II, Acute Physiology and Chronic Health Evaluation II; BISAP, Bedside index of severity in acute pancreatitis; ICU, intensive care unit; MMP9, Matrix metallopeptidase 9; NLRP3, NOD-like receptor thermal protein domain associated protein 3; GSDMD, Gasdermin D; ASC, Apoptosis-associated speck-like protein containing a CARD; Pro caspase-1, Pro-cysteinyl aspartate specific proteinase-1; IL-6, Interleukin-6; IL-18, Interleukin-18; IL-1β, Interleukin-1β; TNF-α, Tumor necrosis factor alpha; ALT, Alanine aminotransferase; AST, Aspartate aminotransferase; Cr, Creatinine; BUN, Blood urea nitrogen; MPO, myeloperoxidase; LPS, Lipopolysaccharide; DAMP, Danger-associated molecular pattern.

Data Sharing Statement

Data sets used and/or analyzed during the current study period are available from corresponding authors upon reasonable request.

Ethics Approval and Consent to Participate

The experimental protocol was approved by the Ethics Committee of Hunan Provincial People's Hospital (Animal Ethics Approval No: 2023-43; Retrospective Study Ethics Approval No: 2024-116). The requirement for informed consent was waived due to the retrospective nature of the study. The study was conducted in accordance with the Declaration of Helsinki, the "Guide for the Care and Use of Laboratory Animals" (8th edition, 2011) published by the National Institutes of Health, and the Regulations on the Administration of Laboratory Animals in the People's Republic of China.

Consent for Publication

All authors critically reviewed the content of the manuscript. The consent for publication was obtained from all authors.

Author Contributions

All authors made a significant contribution to the work reported, whether that is in the conception, study design, execution, acquisition of data, analysis and interpretation, or in all these areas; took part in drafting, revising or critically reviewing the article; gave final approval of the version to be published; have agreed on the journal to which the article has been submitted; and agree to be accountable for all aspects of the work.

Funding

Disclosure

The authors report no conflicts of interest in this work.

References

1. Garg PK, Singh VP. Organ failure due to systemic injury in acute pancreatitis. *Gastroenterology.* 2019;156(7):2008–2023. doi:10.1053/j.gastro.2018.12.041
2. Zhou MT, Chen CS, Chen BC, Zhang QY, Andersson R. Acute lung injury and ARDS in acute pancreatitis: mechanisms and potential intervention. *World J Gastroenterol.* 2010;16(17):2094–2099. doi:10.3748/wjg.v16.i17.2094

3. Liu D, Wen L, Wang Z, et al. The mechanism of lung and intestinal injury in acute pancreatitis: a review. *Front Med Lausanne*. 2022;9:904078. doi:10.3389/fmed.2022.904078

4. Wu J, Zhang J, Zhao J, Chen S, Zhou T, Xu J. Treatment of severe acute pancreatitis and related lung injury by targeting gasdermin D-mediated pyroptosis. *Front Cell Dev Biol*. 2021;9:780142. doi:10.3389/fcell.2021.780142

5. Elder AS, Saccone GT, Dixon DL. Lung injury in acute pancreatitis: mechanisms underlying augmented secondary injury. *Pancreatology*. 2012;12(1):49–56. doi:10.1016/j.pan.2011.12.012

6. Ge P, Luo Y, Yang Q, et al. Ferroptosis in rat lung tissue during severe acute pancreatitis-associated acute lung injury: protection of qingyi decoction. *Oxid Med Cell Longev*. 2023;2023:5827613. doi:10.1155/2023/5827613

7. Zhou J, Zhou P, Zhang Y, Wang G, Fan Z. Signal pathways and markers involved in acute lung injury induced by acute pancreatitis. *Dis Markers*. 2021;2021:9947047. doi:10.1155/2021/9947047

8. Chen W, Yang X, Huang L, et al. Qing-Yi decoction in participants with severe acute pancreatitis: a randomized controlled trial. *Chin Med*. 2015;10(1):11. doi:10.1186/s13020-015-0039-8

9. Wang Z, Liu J, Li F, et al. Mechanisms of qingyi decoction in severe acute pancreatitis-associated acute lung injury via gut microbiota: targeting the short-chain fatty acids-mediated AMPK/NF-κB/NLRP3 pathway. *Microbiol Spectr*. 2023;11(4):e366422. doi:10.1128/spectrum.03664-22

10. Wang G, Shang D, Zhang G, et al. Effects of QingYi decoction on inflammatory markers in patients with acute pancreatitis: a meta-analysis. *Phytomedicine*. 2022;95:153738. doi:10.1016/j.phymed.2021.153738

11. Ma S, Wei T, Zhang B, et al. Integrated pharmacokinetic properties and tissue distribution of multiple active constituents in Qing-Yi Recipe: a comparison between granules and decoction. *Phytomedicine*. 2024;129:155645. doi:10.1016/j.phymed.2024.155645

12. Chinese Pancreatic Surgery Association, Chinese Medical Association. Guidelines for diagnosis and treatment of acute pancreatitis in China (2021). *Zhonghua Wai Ke Za Zhi*. 2021;59(7):578–587. doi:10.3760/cma.j.cn112139-20210416-00172

13. Nesvaderani M, Dhillon BK, Chew T, et al. Gene expression profiling: identification of novel pathways and potential biomarkers in severe acute pancreatitis. *J Am Coll Surg*. 2022;234(5):803–815. doi:10.1097/XCS.0000000000000115

14. Ritchie ME, Phipson B, Wu D, et al. limma powers differential expression analyses for RNA-sequencing and microarray studies. *Nucleic Acids Res*. 2015;43(7):e47. doi:10.1093/nar/gkv007

15. Wang Z, Liu J, Wang Y, et al. Identification of key biomarkers associated with immunogenic cell death and their regulatory mechanisms in severe acute pancreatitis based on WGCNA and machine learning. *Int J mol Sci*. 2023;24(3):3033. doi:10.3390/ijms24033033

16. Yang R, Yang H, Wei J, et al. Mechanisms underlying the effects of lianhua qingwen on sepsis-induced acute lung injury: a network pharmacology approach. *Front Pharmacol*. 2021;12:717652. doi:10.3389/fphar.2021.717652

17. Saad MI, Jenkins BJ. An in vitro model for assessing acute lung injury during pancreatitis development using primary mouse cell co-cultures. *Methods mol Biol*. 2023;2691:71–80. doi:10.1007/978-1-0716-3331-1_6

18. Zhou P, Song NC, Zheng ZK, Li YQ, Li JS. MMP2 and MMP9 contribute to lung ischemia-reperfusion injury via promoting pyroptosis in mice. *BMC Pulm Med*. 2022;22(1):230. doi:10.1186/s12890-022-02018-7

19. Rashad S, Niizuma K, Sato-Maeda M, et al. Early BBB breakdown and subacute inflammasome activation and pyroptosis as a result of cerebral venous thrombosis. *Brain Res*. 2018;1699:54–68. doi:10.1016/j.brainres.2018.06.029

20. Yadav SK, Kambis TN, Kar S, Park SY, Mishra PK. MMP9 mediates acute hyperglycemia-induced human cardiac stem cell death by upregulating apoptosis and pyroptosis in vitro. *Cell Death Dis*. 2020;11(3):186. doi:10.1038/s41419-020-2367-6

21. Bellut M, Papp L, Bieber M, Kraft P, Stoll G, Schuhmann MK. NLPR3 inflammasome inhibition alleviates hypoxic endothelial cell death in vitro and protects blood-brain barrier integrity in murine stroke. *Cell Death Dis*. 2021;13(1):20. doi:10.1038/s41419-021-04379-z

22. Liu B, Li N, Liu Y, et al. BRD3308 suppresses macrophage oxidative stress and pyroptosis via upregulating acetylation of H3K27 in sepsis-induced acute lung injury. *Burns Trauma*. 2024;12:tkae33. doi:10.1093/burnst/tkae033.

23. Egorov D, Kopaliani I, Ameln AK, Speier S, Deussen A. Mechanism of pro-MMP9 activation in co-culture of pro-inflammatory macrophages and cardiomyocytes. *Exp Cell Res*. 2024;434(1):113868. doi:10.1016/j.yexcr.2023.113868

24. Lei H, Minghao W, Xiaonan Y, Ping X, Ziqi L, Qing X. Acute lung injury in patients with severe acute pancreatitis. *Turk J Gastroenterol*. 2013;24(6):502–507. doi:10.4318/tjg.2013.0544

25. Sarr MG, Banks PA, Bollen TL, et al. The new revised classification of acute pancreatitis 2012. *Surg Clin North Am*. 2013;93(3):549–562. doi:10.1016/j.suc.2013.02.012

26. Schepers NJ, Bakker OJ, Besselink MG, et al. Impact of characteristics of organ failure and infected necrosis on mortality in necrotising pancreatitis. *Gut*. 2019;68(6):1044–1051. doi:10.1136/gutjnl-2017-314657

27. Vege SS, DiMagno MJ, Forsmark CE, Martel M, Barkun AN. Initial medical treatment of acute pancreatitis: American gastroenterological association institute technical review. *Gastroenterology*. 2018;154(4):1103–1139. doi:10.1053/j.gastro.2018.01.031

28. Guo XJ, Guo WB. A clinical study of qingyi decoction in the treatment of acute pancreatitis. *J Biol Regul Homeost Agents*. 2019;33(4):1197–1200.

29. Ji CH, Tang CW, Feng WM, Bao Y, Yao LQ. A Chinese herbal decoction, huoxue qingyi decoction, promotes rehabilitation of patients with severe acute pancreatitis: a retrospective study. *Evid Based Complement Alternat Med*. 2016;2016:3456510. doi:10.1155/2016/3456510

30. Li L, Li YQ, Sun ZW, et al. Qingyi decoction protects against myocardial injuries induced by severe acute pancreatitis. *World J Gastroenterol*. 2020;26(12):1317–1328. doi:10.3748/wjg.v26.i12.1317

31. Wei TF, Zhao L, Huang P, et al. Qing-Yi decoction in the treatment of acute pancreatitis: an integrated approach based on chemical profile, network pharmacology, molecular docking and experimental evaluation. *Front Pharmacol*. 2021;12:590994. doi:10.3389/fphar.2021.590994

32. Zhang D, Li L, Li J, et al. Colchicine improves severe acute pancreatitis-induced acute lung injury by suppressing inflammation, apoptosis and oxidative stress in rats. *Biomed Pharmacother*. 2022;153:113461. doi:10.1016/j.biopha.2022.113461

33. Hu Q, Yao J, Wu X, et al. Emodin attenuates severe acute pancreatitis-associated acute lung injury by suppressing pancreatic exosome-mediated alveolar macrophage activation. *Acta Pharm Sin B*. 2022;12(10):3986–4003. doi:10.1016/j.apsb.2021.10.008

34. Kong L, Deng J, Zhou X, et al. Sitagliptin activates the p62-Keap1-Nrf2 signalling pathway to alleviate oxidative stress and excessive autophagy in severe acute pancreatitis-related acute lung injury. *Cell Death Dis*. 2021;12(10):928. doi:10.1038/s41419-021-04227-0

35. Vande WL, Lamkanfi M. Drugging the NLRP3 inflammasome: from signalling mechanisms to therapeutic targets. *Nat Rev Drug Discov*. 2024;23(1):43–66. doi:10.1038/s41573-023-00822-2

36. Xia S, Gu X, Wang G, et al. Regulated cell death of alveolar macrophages in acute lung inflammation: current knowledge and perspectives. *J Inflamm Res*. 2024;17:11419–11436. doi:10.2147/JIR.S497775

37. Shen X, He L, Cai W. Role of lipopolysaccharides in the inflammation and pyroptosis of alveolar epithelial cells in acute lung injury and acute respiratory distress syndrome. *J Inflamm Res*. 2024;17:5855–5869. doi:10.2147/JIR.S479051

38. Tong Y, Bao C, Xu YQ, et al. The β3/5 Integrin-MMP9 axis regulates pulmonary inflammatory response and endothelial leakage in acute lung injury. *J Inflamm Res*. 2021;14:5079–5094. doi:10.2147/JIR.S331939

39. Liu C, Xi L, Liu Y, et al. An inhalable hybrid biomimetic nanoplatform for sequential drug release and remodeling lung immune homeostasis in acute lung injury treatment. *ACS Nano*. 2023;17(12):11626–11644. doi:10.1021/acsnano.3c02075

40. Zhang F, Hu L, Wu YX, et al. Doxycycline alleviates paraquat-induced acute lung injury by inhibiting neutrophil-derived matrix metalloproteinase 9. *Int Immunopharmacol*. 2019;72:243–251. doi:10.1016/j.intimp.2019.04.015

41. Zhang H, Mao YF, Zhao Y, et al. Upregulation of matrix metalloproteinase-9 protects against sepsis-induced acute lung injury via promoting the release of soluble receptor for advanced glycation end products. *Oxid Med Cell Longev*. 2021;2021(1):8889313. doi:10.1155/2021/8889313

42. Tong Y, Yu Z, Chen Z, et al. The HIV protease inhibitor Saquinavir attenuates sepsis-induced acute lung injury and promotes M2 macrophage polarization via targeting matrix metalloproteinase-9. *Cell Death Dis*. 2021;12(1):67. doi:10.1038/s41419-020-03320-0

43. Keck T, Jargon D, Klünsch A, et al. MMP-9 in serum correlates with the development of pulmonary complications in experimental acute pancreatitis. *Pancreatology*. 2006;6(4):316–322. doi:10.1159/000092797

44. Vitale DS, Lahni P, Hornung L, et al. Matrix metalloproteinases and their inhibitors in pediatric severe acute pancreatitis. *PLoS One*. 2022;17(2): e261708. doi:10.1371/journal.pone.0261708

45. Li D, Liu S, Lu X, et al. The circadian clock gene bmal1 regulates microglial pyroptosis after spinal cord injury via NF-κB/MMP9. *CNS Neurosci Ther*. 2024;30(12):e70130. doi:10.1111/cns.70130

46. Jia SY, Yin WQ, Xu WM, Li J, Yan W, Lin JY. Liquiritin ameliorates painful diabetic neuropathy in SD rats by inhibiting NLRP3-MMP-9-mediated reversal of aquaporin-4 polarity in the glymphatic system. *Front Pharmacol*. 2024;15:1436146. doi:10.3389/fphar.2024.1436146

47. Fan H, Tian H, Jin F, et al. CypD induced ROS output promotes intracranial aneurysm formation and rupture by 8-OHdG/NLRP3/MMP9 pathway. *Redox Biol*. 2023;67:102887. doi:10.1016/j.redox.2023.102887